Dielectric and structural properties of aqueous nonpolar solute mixtures

I. Shvab and Richard J. Sadus[a)]
Centre for Molecular Simulation, Swinburne University of Technology, PO Box 218 Hawthorn, Victoria 3122, Australia

The dielectric properties and molecular structure of water mixtures with different nonpolar solutes (methane and noble gases) are studied using molecular dynamics. The water-water, water-solute, and solute-solute interactions are calculated using the combination of a polarizable potential [J. Li, Z. Zhou, and R. J. Sadus, J. Chem. Phys. **127**, 154509 (2007)] for water plus the Lennard-Jones potential. The effect of solute size and concentration on the solubility of the system, hydrogen bonding, dielectric constant, and dipole moment are investigated over a temperature range of 278–750 K and solute percentage mole fractions up to 30%. Solute particles affect the structure of water, resulting in the compression of oxygen-oxygen and oxygen-hydrogen radial distribution functions. The influence of the solute extends both to relatively low concentrations and high temperatures. The coordination numbers of aqueous solutions of the nonpolar solutes appear to be proportional to the size of the solute particles. Our study shows the destructive influence of the nonpolar solute on both the tetrahedral water structure and hydrogen bond formation at solute concentrations greater than 30%. The presence of nonpolar particles typically decreases both the dielectric constant and dipole moment. The decrease of dielectric constant and water dipole moment is directly proportional to the solute concentration and temperature. © *2012 American Institute of Physics*. [http://dx.doi.org/10.1063/1.4753940]

I. INTRODUCTION

Binary fluid systems of water and an inert nonpolar second component have been extensively investigated experimentally[1–5] and with the help of molecular dynamics (MD) and Monte Carlo (MC) techniques. Phase equilibria, critical curves, and thermodynamics functions for a wide range of temperatures and pressures have been determined for mixtures containing water plus argon,[1] xenon,[2] neon,[3] and methane,[4] etc. Aqueous mixtures are of considerable interest in geochemistry and chemical technology (development of undersea deposits of gas hydrates), industrial technology (electric power generation, extraction process, decontamination), and biochemistry (protein folding, micellization). In particular, the solvation of nonpolar gases exhibits interesting behavior with increasing temperature. The solubility of inert gases in water at room temperature, which is several orders of magnitude smaller than in other liquids such as hydrocarbons, initially decreases with increasing temperature, goes through a minimum, and then exhibits a steep rise at subcritical temperatures. Complete miscibility is eventually reached for several nonpolar molecules above the critical temperature of water. This makes supercritical water a useful medium for chemical reactions.

Despite the importance of supercritical aqueous mixtures, the molecular structure of supercritical water in the presence of nonpolar solutes has not been extensively determined experimentally. Recent neutron diffraction studies explored the hydration shell of argon at sub-critical conditions, using distinct isotopes of argon in normal and heavy water.[5,6]

These data showed structural changes in the hydration shell of the solute, compared to ambient conditions, in agreement with previous MD simulations on mixtures of rare gases and extended simple point charge (SPC/E) water.[7,8] In the presence of a nonpolar solute, reorganization of the water solvent is observed[5–7] around the hydrophobic solute molecules. The ordering of water causes a decrease of entropy in competition with the enthalpic term, which favors solvation. The nonpolar molecules of the solute tend to aggregate to reduce the local order of the water molecules. The balance between the entropic and the enthalpic terms determines the phenomenon of hydrophobic hydration.[7,9] It has also been observed that the solubility of rare gases increases as the size of the solute increases,[7,10,11] which is attributed to the interplay between energetic and entropic contributions to the free energy of solvation. According to the simulation results reported by Guillot and Guissani[7] with the SPC/E model,[12] the energetic term favors the solubility of larger solutes while the entropic term depresses solubility with increasing size.

The question of the solubility of nonpolar particles in water is directly relevant to the formation of clathrate hydrates.[13] Clathrate hydrates are supramolecular compounds of water molecules and guest components without chemical bonds between them. Water molecules form a three-dimensional host structure (the lattice) through hydrogen bonding; this lattice is at sufficiently low density to contain a number of well-characterized pores, or "cages," in which other molecules (guests) are trapped. It is reported that, despite being chemically neutral, most of the noble gases form clathrates in water.[14] The conditions for clathrate hydrate formation depend on temperature, pressure, and the concentration of the solute. Therefore, the knowledge of solute concentrations

---

[a)]Electronic mail: rsadus@swin.edu.au.

137, 124501-1

at which the "cages" are stable is of great importance. Undoubtedly, among the many clathrate hydrates, methane clathrates are of paramount interest for modern industry.

Methane is the simplest hydrocarbon molecule and has often been considered to be a good model for understanding hydrophobic interactions. It is now generally believed that the nature of hydrophobicity is size dependent. Small nonpolar molecules such as methane have a hydration free energy near ambient conditions that is largely entropic; that is, it depends more on the number of ways all of the water molecules in the methane hydration shell can form hydrogen bonds rather than their energies. Therefore, the number of water molecules in the solvation shell of small nonpolar molecules is of central importance.

Another interesting effect of nonpolar solutes is their influence on the polarization properties of water. The polarization properties of critical and supercritical water in the presence of nonpolar solutes have not been determined experimentally. Polarizable potentials were used in the molecular simulation studies of Cristofori et al.[11] and Dyer et al.[15] and references therein. However, these studies were devoted mainly to the question of the solubility of nonpolar solutes in water at very low concentrations.

The main aim of this work is to use molecular simulation to investigate the structure of water-nonpolar systems at ambient, critical, and supercritical temperatures and solute mole fractions up to 30%. Previous studies were unable to indicate how the hydration number might vary with the temperature and pressure at which the hydrate was formed. This work provides data for the hydration number over a wide range of state points for water plus noble gases and methane. Results are reported for the solvation shell size, hydration number, and role of the solute particle size on solubility of the solute and their temperature dependence. The dipole moment and dielectric constant of water-nonpolar solute systems are also investigated.

II. THEORY

A. Intermolecular potentials

1. Water-water potential

In this work, we investigate the influence of nonpolar solute concentrations and size on structural and polarization properties of water in the temperature range of 278–750 K. We consider water molecules as a rigid triatomic system with two negative charges placed on hydrogen atoms and one positive charge placed on the bisector of the H–O–H angle near the oxygen atom. The geometry of the water molecule is the same as given in Ref. [16] with an O–H bond length of 0.9572 Å and a H–O–H bond angle of 104.52°. For the calculation of water-water intermolecular interactions, we have used the polarizable Matsuoka-Clementi-Yoshimine nonadditive (MCYna) potential[17] model which originates from the *ab initio* Matsuoka-Clementi-Yoshimine (MCY) potential.[16] The intermolecular potential $U(r)$ for water is the sum of two-body additive u_2, nonadditive three-body u_3, and polarizable u^{pol}

TABLE I. Intermolecular parameters used in the MCYna[17] intermolecular potential. Unless otherwise stated, all values are in atomic units.

Parameter	Value
a_1	1734.1960
a_2	2.726696
a_3	1.061887
a_4	1.460975
b_1	2.319395
b_2	1.567367
b_3	0.436060
b_4	1.181792
q^2	0.514783
r_{OH}	0.957200
r_{OM}	0.505783
θ_{HOH} (deg)	104.52
α (Å^3)	1.44
ν	287.944

contributions

$$U(\vec{r}) = \sum_{i<j}^{N} u_2(\vec{r}_i, \vec{r}_j) + \sum_{i<j<k}^{N} u_3(\vec{r}_i, \vec{r}_j, \vec{r}_k) + u^{pol}. \quad (1)$$

The contribution of two-body interactions was obtained from the *ab initio* MCY potential,[16]

$$u_2 = q^2 \cdot \left(\frac{1}{r_{13}} + \frac{1}{r_{14}} + \frac{1}{r_{23}} + \frac{1}{r_{24}} \right) + \frac{4q^2}{r_{78}}$$
$$- 2q^2 \left(\frac{1}{r_{18}} + \frac{1}{r_{28}} + \frac{1}{r_{37}} + \frac{1}{r_{47}} \right) + a_1 e^{(-b_1 r_{56})}$$
$$+ a_2 (e^{(-b_2 r_{13})} + e^{(-b_2 r_{14})} + e^{(-b_2 r_{23})} + e^{(-b_2 r_{24})})$$
$$+ a_3 (e^{(-b_3 r_{16})} + e^{(-b_3 r_{26})} + e^{(-b_3 r_{35})} + e^{(-b_3 r_{45})})$$
$$- a_4 (e^{(-b_4 r_{16})} + e^{(-b_4 r_{26})} + e^{(-b_4 r_{35})} + e^{(-b_4 r_{45})}). \quad (2)$$

The meaning of the parameters is the same as given in the literature[16] and their values are summarized in Table I. The various distances used in Eq. (2) are defined in Fig. 1. The benefit of an *ab initio* potential is that it should avoid many of the theoretical uncertainties of empirical intermolecular
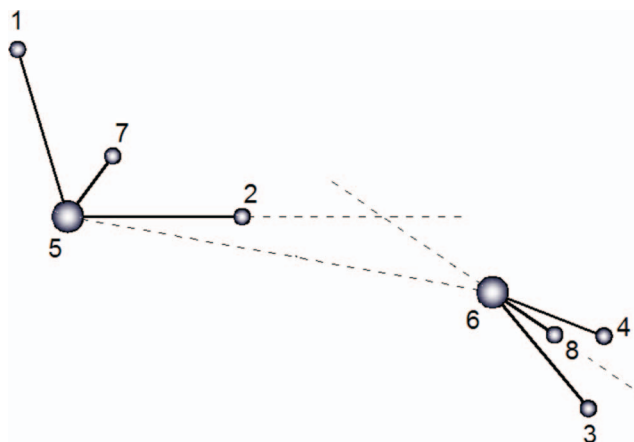

FIG. 1. Definition of the water dimer geometry identifying the intermolecular separations used in the two-body contribution to the MCYna potential appearing in Eq. (2).

potentials, such as the need to fit the parameters of the potential to experimental data for various properties.

Nonadditive contributions to intermolecular interactions arise for induction interactions, resulting from molecular polarizability, short-range repulsion, and dispersion interactions. It is well documented[17,18] that multibody dispersion interactions can be adequately described using the Axilrod-Teller[19] triple dipole term,

$$u_3 = \frac{\nu(1 + 3\cos\theta_i \cos\theta_j \cos\theta_k)}{(r_{ij}r_{ik}r_{jk})^3}, \qquad (3)$$

where θ_i, θ_j, and θ_k are inside angles of the triangle formed by three atoms denoted by i, j, and k, and r_{ij}, r_{ik}, and r_{jk} are the three side lengths of the triangle. Equation (3) is applied exclusively for triplets of oxygen atoms because their positions almost coincide with the center of the mass of the water molecule and the three-body interaction between hydrogen atoms is negligible by comparison. The parameter ν is the nonadditive coefficient, which can be determined from experiment.[20] The theoretical background and rationale for using this formula is given elsewhere.[17] The contribution of multibody nonadditive from polarization interactions was obtained from[21]

$$u^{pol} = -\frac{1}{2}\sum_{i=1}^{N} \vec{\mu}_i^{ind} \cdot \vec{E}_i^o, \qquad (4)$$

where $\vec{E}_i^o$ is the electrostatic field of surrounding charges, and $\vec{\mu}_i^{ind}$ is the induced dipole at site i given by

$$\vec{\mu}_i^{ind} = \alpha\beta \cdot \vec{E}_i = \alpha\beta \cdot \left[\vec{E}_i^o + \sum_{j=1, j \neq i}^{N} T_{ij}\vec{\mu}_j^{ind} \right]. \qquad (5)$$

In Eq. (5), $\alpha\beta$ is the polarizability and $\boldsymbol{T_{ij}}$ is the dipole tensor given by

$$T_{ij} = \frac{1}{4\pi\varepsilon_o r_{ij}^5}\left[3r_{ij}r'_{ij} - r_{ij}^2\right]. \qquad (6)$$

2. Water-solute and solute-solute potentials

For the MD simulations, we consider solute particles as points with zero charge. Due to the weak interaction between water and noble gases, which can serve as a model for hydrophobic interactions of water with nonpolar particles, the exact form of the interaction potential is still not known. Many early *ab initio* and MD simulation were performed to determine the form of this potential for water-Ne,[22] water-Ar,[22,23] water-Kr, and water-Xe[15] interactions. However, such *ab initio* potentials[22,23] are very computationally expensive or were applied for the case of very dilute solutions.[15] In addition to their theoretical complexity, the common disadvantage of these *ab initio* potentials is their inability to reproduce London dispersion interactions. In this work, for the sake of simplicity and computational economy, we have used the Lennard-Jones (LJ) potential to handle interactions between water and solute

TABLE II. Lennard-Jones potential parameters used for water-solute and solute-solute pair interactions.[7]

	ε/k_b (K)	σ (nm)
H_2O	78.22	0.31366(O)
Ne	18.56	0.3035
Ar	125.0	0.3415
CH_4	147.5	0.3730
Kr	169.0	0.3675
Xe	214.7	0.3975

particles

$$u_{ij} = 4\varepsilon\left[\left(\frac{\sigma}{r_{ij}}\right)^{12} - \left(\frac{\sigma}{r_{ij}}\right)^{6}\right], \qquad (7)$$

where σ is the atomic diameter and ε is the well depth. We have chosen the parameters (see Table II) of the LJ potential that are appropriate for solute particles of neon, argon, krypton, xenon, and methane.[7] It is well established that the Lennard-Jones potential is a reasonable approximation for the intermolecular interactions of argon, krypton, and xenon. In contrast, increasing quantum influences mean that the parameterization of the potential for neon is likely to be less accurate. Although calculations for mixtures including neon are likely to be less quantitatively accurate than for the other systems, the trends observed are likely to be at least qualitatively correct. Calculations for water-neon are also reported here for the benefit of completeness.

The interactions between methane and water molecules stand out because of the polyatomic structure of the methane molecule. The real water-methane energy surface is not isotropic in relation to all possible mutual orientations of interacting molecules.[24] For example, as was shown by Mateus *et al.*,[25] the two most common configurations are the ones were methane plays the role of either proton acceptor, or proton donor. Consequently each configuration has different probability and energy. Nonetheless, the Lennard-Jones potential has been commonly used to represent methane with considerable success.[6,13] For the purposes of this work, we can easily apply the LJ potential for water-methane and methane-methane interactions. LJ parameters are given in Table II. Parameters for water-solute interaction are defined by the Lorentz-Berthelot combining rules

$$\sigma_{12} = \frac{\sigma_1 + \sigma_2}{2}, \qquad (8)$$

$$\varepsilon_{12} = \sqrt{\varepsilon_1 \cdot \varepsilon_2}. \qquad (9)$$

As long as hydrogen atoms have zero ε and σ, only oxygen atoms participate in direct LJ interaction with solute particles.

B. Properties calculated

1. Structural properties

The structure of water was investigated by calculating the radial distribution function (RDF) $g(r)$ from the

following formula:[21]

$$g_{ij}(r) = \frac{V}{4\pi\rho^2 N(N-1)} \left\langle \sum_i n_i(r)\Delta r \right\rangle, \qquad (10)$$

where V is the system volume, and $n(r)\Delta r$ is the number of particles that exist in the region between r and $r + \Delta r$. For polyatomic molecules, all the different combinations of RDFs give relative positions of molecules as well as the intermolecular bonding information. We also calculated the first solute-oxygen, oxygen-oxygen, and oxygen-hydrogen coordination numbers,

$$n_{ij} = 4\pi\rho \int_0^{r_{\min}} g_{ij}(r) r^2 dr, \qquad (11)$$

where ρ is the number density, which in this work is equal to 100 particles/nm^3. The ij subscript in $g_{ij}(r)$ stands for different kinds of interatomic RDFs we are interested in; for example, O–H, O–O, Ne–O, Ar–O, CH$_4$–O, etc.

2. Dielectric constant and dipole moment

The dielectric constant or relative permittivity ε_m is directly related to the intermolecular orientational correlation and magnitude of each molecular dipole moment. The dielectric constant was calculated in these simulations from the total dipole moment fluctuation,[21,26]

$$\varepsilon_m = 1 + \frac{4\pi\rho\mu^2}{3k_B T} g_k. \qquad (12)$$

In Eq. (12), k_B is the Boltzmann constant, and g_k is the Kirkwood factor, which can be obtained from the fluctuation of the total dipole moment $[\vec{M} = \sum (\vec{\mu}_i + \vec{\mu}_i^{ind})]$ of the ensemble,

$$g_k = \frac{\langle M^2 \rangle}{N\mu^2}. \qquad (13)$$

The Kirkwood factor is defined such that it has a value of unity if no orientational correlation is found. For a water-solute system, the total dipole moment should contain contributions from all species[27]

$$M^2 = \sum x_i M_i^2 = x_s M_s^2 + x_w M_w^2, \qquad (14)$$

where x_s and x_w are mole fractions of solute and water, respectively. Because the nonpolar solute particles do not have a permanent dipole moment, only water molecules contribute to the total dipole moment of the system. The evaluation of ε_m depends on the treatment of the long-range electrostatic interactions. The Ewald sum was used for long-range electrostatic interactions in the dielectric constant calculation, which is equivalent to tin-foil boundary conditions in the reaction field method (see Ref. 17 and references therein). As discussed elsewhere,[28] this approximation introduces an additional uncertainty in the results. However, in practice the reported errors[17] are negligible. The total molecular dipole moment $\vec{\mu}$, which has contributions from both the partial charge (permanent electric dipole equals 2.1936 D) and the induction

interactions, is averaged over the entire ensemble,

$$\vec{\mu} = \frac{1}{N} \sum_{i=1}^N (\vec{\mu}_i + \vec{\mu}_i^{ind}). \qquad (15)$$

C. Simulation details

Canonical NVT molecular dynamics simulations using the Shake algorithm[26] were performed for systems of N = 500 particles with a density 1.0 g/cm^3 and a temperature range of 278–750 K. Several MD simulations were performed for systems with solute percentage mole fractions of x_s = 1%, 2%, 4%, 6%, 10%, 15%, 20%, and 30%. The Ewald summation method was used to evaluate the long-range part of the Coulomb potential.[26] The convergence parameter for the Ewald sum was $\alpha = 5.0/L$, with summation over $5 \times 5 \times 5$ reciprocal lattice vectors, where L is the box length. The three-body interactions were truncated at $L/4$,[18] and a cutoff of $L/2$, is applied to the additive two-body interaction. During the pre-equilibration stage, the temperature was held constant by rescaling the velocities every ten steps, which we found to be equivalent to results obtained using a Gaussian thermostat. The simulations were commenced from an initial face centered cubic lattice with a time step of 2 fs. The systems were equilibrated for 500 ps before any ensemble averages were determined. At each temperature, the total simulation time was at least 2 ns, which corresponds to 1×10^6 time steps. The equations of motion were integrated using a leap-frog algorithm.[26] To determine the induced dipole moment, a direct solver, namely, the conjugate gradient method[29] was used. To speed up the calculations of the dielectric constant, which is slow to converge, the first 500 ps of the simulation was performed without the Axilrod-Teller term. In this case, the total simulation time was 2 ns. Ensemble averages were obtained by analyzing post-equilibrium configurations at intervals of 100 time steps and standard deviations were determined.

III. RESULTS AND DISCUSSION

A. Water-solute radial distribution functions

To define the inner structure of these systems, we studied RDFs at 298 K and $x_s = 20\%$ for Ne and Ar, $x_s = 15\%$ for CH$_4$, $x_s = 10\%$ for Kr, and 6% for Xe. Figure 2 shows solute-oxygen (g_{so}) radial distribution functions. From this figure, we can see that the solute-oxygen curves start at distances proportional to the parameter σ, in the following order $\sigma_{Ne} < \sigma_{Ar} < \sigma_{CH4} < \sigma_{Kr} < \sigma_{Xe}$. The position of the 1st peak allows us to identify the radius of the 1st solvation shell water molecules formed around solute particles. The approximate radii for the given values of x_s and temperature are: $r_{Ne} = 0.313$, $r_{Ar} = 0.332$, $r_{CH4} = 0.334$, $r_{Kr} = 0.35$, and $r_{Xe} = 0.365$ nm. Simulations performed for higher temperatures show that the size of the solvation shells decrease slightly with increasing temperature.

One of the main tasks of the present work was to investigate the distortion of the structure of water caused by the inert solutes. Figure 3 compares oxygen-oxygen (g_{oo}), oxygen-hydrogen (g_{oh}), and hydrogen-hydrogen (g_{hh}) RDFs
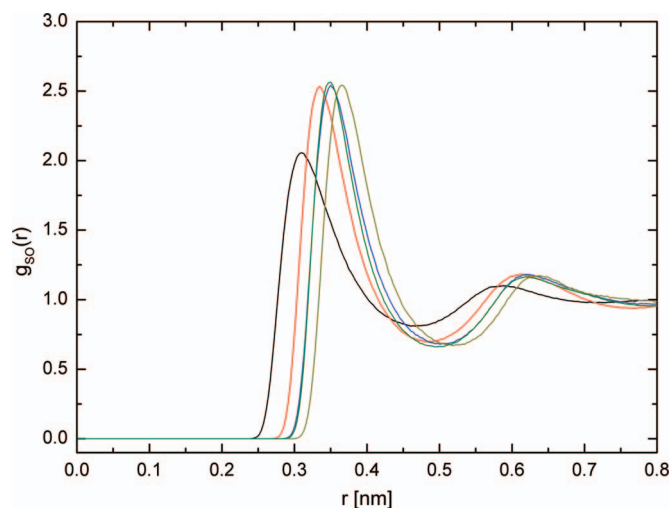
FIG. 2. Solute-oxygen $g_{so}(r)$ radial distribution functions for water-solute systems at 298 K. Starting from left to the right, the solutes are Ne (black x_S = 20%), Ar (red x_S = 20%), CH$_4$ (green x_S = 15%), Kr (blue x_S = 10%), and Xe (olive x_S = 6%).

for pure water with RDFs of water-Ne, water-Ar, and water-CH$_4$ systems at T = 298 K and x_s = 20%. It is apparent from Fig. 3 that the presence of the nonpolar solute increases and slightly widens the 1st O–O, O–H, and H–H peaks. Water-
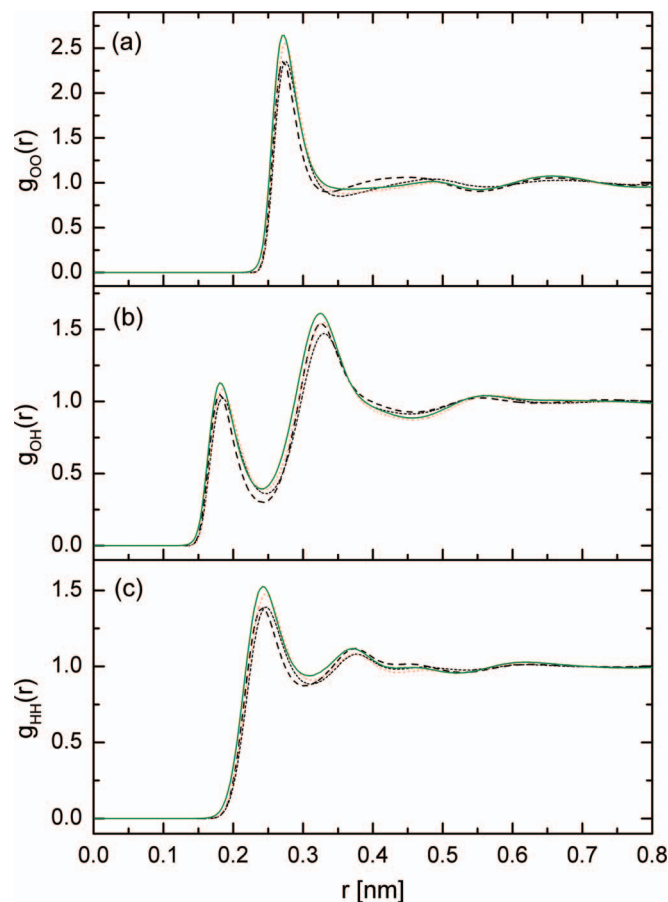
FIG. 3. (a) Oxygen-oxygen $g_{oo}(r)$, (b) oxygen-hydrogen $g_{oh}(r)$, and (c) hydrogen-hydrogen $g_{hh}(r)$ distribution functions of pure water (dashed black line) and aqueous solutions of Ne (short dashed line x_S = 20%), Ar (dotted red line x_S = 20%), and CH$_4$ (continuous green line x_S = 15%) at T = 298 K.

argon and water-methane O–O and O–H first peaks are higher than in the case of pure water (dashed curve). We can conclude that increasing the concentration of a large nonpolar solute particle such as Ar or CH$_4$ compresses the water structure because of solute-oxygen repulsion. The second O–O peak is flattening out and almost disappears in the presence of 15%–20% solute particles, which indicates a significant distortion of the usual water shell structure by solute particles at distances larger than 0.4 nm. The effect of the solutes on $g_{oh}(r)$ is to increase the 1st minima and decrease the 2nd minima. In general, data from Fig. 3 suggest that the solute particles slightly distort the 1st shell while the distortion of water structure at longer distances is much more significant. Similar indications of nonpolar solutes induced distortion of water structure were obtained for dilute aqueous mixtures of Ar,[6,30] CH$_4$,[31] He,[6] and Kr.[6]

By analyzing the distribution functions from Figs. 2 and 3, we can infer the shape of the solvation shell around solute particles. For example, by comparing the 1st Ne–O and Ne–H peaks positions, we can see that the 1st Ne–H peak is located some 0.95 nm closer to the Ne atom than the 1st Ne–O peak, which is almost equal to the length of O–H covalent bond (0.9752 nm for the MCYna model). Taking this into account, we can infer that the hydrogen atoms of the water molecules, which form a shell around Ne atoms, are oriented almost radially inward. This orientation of H-atoms is in agreement with the Hartree-Fock calculations of Losonczy *et al.*,[22] which indicate that the water-neon pair potential has a minimum when the Ne atom is located in the water molecule plane along one of the O–H axes. RDFs for larger solute particles show similar behavior. The hydrogen atoms of water molecules in the 1st solvation shell are orientated slightly toward the central solute particle, and not almost completely radially as is the case for the small Ne atom.

The 2nd peaks of $g_{ArO}(r)$, $g_{CH_4-O}(r)$, $g_{KrO}(r)$, and $g_{XeO}(r)$ are located at a shorter distance than the 2nd peaks of the corresponding solute-hydrogen functions (0.615 nm for Ar–O vs. 0.64 nm for Ar–H, 0.638 nm for CH$_4$–O vs. 0.66 nm for CH$_4$–H, 0.62 nm for Kr–O vs. 0.665 nm for Kr–H, and 0.583 nm for Xe–O vs. 0.63 nm for Xe–H for the values of x_s indicated in Fig. 2). This means that the water molecules of the 2nd shell point their oxygen atoms preferentially toward the solute and the hydrogen atoms toward the bulk, while in the 1st shell H atoms are pointed from the bulk and toward the solute particle. This enclathration mechanism, or encagement phenomenon, has been viewed in several simulation studies[7,8,11,30] on hydrophobic solutes in water and it is one of the most important features of hydrophobic hydration at the atomic level.

B. One-phase region

Solute concentration and size also affect the solubility of the given substances in water. Our simulations indicate a tendency for the large Xe and Kr atoms to demix at concentrations higher than 6% and 10%, respectively. Medium sized Ar and CH$_4$ tend to demix at $x_s > 30$% while small Ne atoms remain in a single phase with water even at higher concentrations. The solubility of these particles also depends on temperature. At $x_s \leq 10$%, all the water-solutes systems

appear to be in one phase throughout the entire temperature region of 278–750 K irrespective of the size of the solute particles. At ambient temperatures, both water-Ar and water-CH$_4$ systems separated into two phases when x_s = 20%. At x_s = 30%, water-Ar and water-CH$_4$ systems do not tend to mix at temperatures up to 340 K and 450 K, respectively. Therefore, all results presented in the given work belong to the ranges of x_s and temperature where full water-solute miscibility is attained.

We report calculations for the homogeneous phase at elevated temperatures, involving solute concentrations up to 30%. These phase conditions obtained at constant volume (NVT ensemble) should not be confused with the very small solubility of noble gases and methane in water at ambient conditions. Extensive experimental studies of various aqueous solutions of nonpolar solutes conducted by Franck et al.[1–3] confirm the existence of a single homogeneous phase at x_s = 30% and even higher concentrations at near critical and supercritical temperatures. For example, Fig. 10 in Ref. [32] and Fig. 2 in Ref. [1] show phase equilibrium isopleths and isotherms at solute concentrations up to 30% at near critical temperatures for water-methane and water-argon systems, respectively.

Although the existence of a single phase for water mixtures of relatively high non-polar solute concentrations ($x_s \geq$ 30%) has been observed experimentally at high temperatures and high pressures, the extent of miscibility at low temperatures (T < 500 K) and high pressures remains unclear. The very low methane solubility in water at T < 500 K and p < 100 MPa has been amply demonstrated by both experimental[1–3,33] and simulation data.[4] However, most measurements[33] have been reported for the methane in the gas state, e.g., a density of 0.00068 g/cm^3 at T = 288 K, p = 0.1 MPa. In contrast, for the NVT simulations reported here, the density of the whole mixture is held constant at 1g/cm^3, which is more than 1000 times larger than reported by Zheng et al.[33] and Errington et al.[4] As a result of this confinement, the pressures observed in our simulations are much higher, resulting in increased solubility. For example, our pressures at the same methane concentrations reported in Ref. [4] (Figs. 3–5) are greater than 200 MPa (423 K), 420 MPa (523 K), and 600 MPa (603 K). This compares with pressures less than 100 MPa at low methane concentration at these temperatures.[4] In Ref. [34] (Fig. 2), a schematic pressure-composition diagram for methane + water is reported based on some experimental observations at 298 K. This largely qualitative phase diagram identifies a single-phase liquid region at pressures up to 1 GPa with increasing methane concentration.

To check the stability of the mixtures, we conducted additional simulations for water-Ne and water-CH$_4$ at x_s = 20% and 30% using boxes elongated two-fold in one direction with the clearly separated water-rich and solute-rich phases. We also compared the miscibility range of the MCYna + LJ system with that of the nonpolarizable SPC/E (Ref. [12]) + LJ model. In the elongated simulation box, all systems were equilibrated for 1 ns with another 1 ns dedicated for accumulation of ensemble averages. All systems showed the same mixing behavior as in the original cubic simulation box with the same values of dielectric constant and dipole moment.
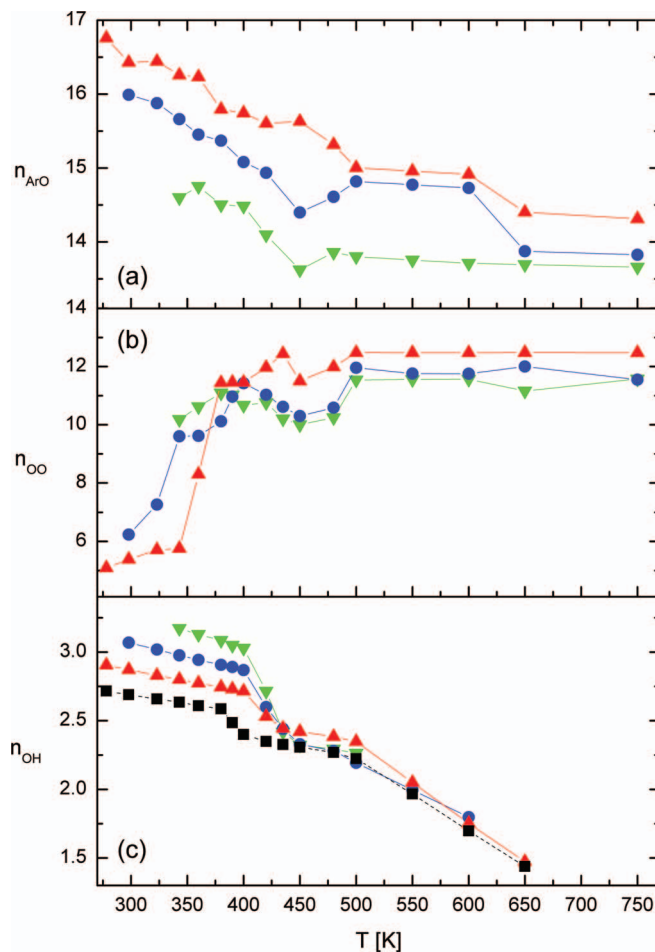

FIG. 4. Temperature dependence of (a) argon-oxygen, (b) oxygen-oxygen, and (c) oxygen-hydrogen coordination numbers at argon mole fractions of 0% (black ■), 10% (red ▲), 20% (blue ●), and 30% (green ▼). The lines through data points are given only for guidance.

We found that the single homogeneous phase for the nonpolarizable SPC/E + LJ system is restricted to smaller solute concentrations than can be observed for the MCYna + LJ system. For water-CH$_4$, the highest solute concentrations at which a single phase was obtained using SPC/E + LJ are x_s = 20% at T > 650 K and x_s = 15% at T > 400 K. For the water-Ne system, the highest single-phase conditions are x_s = 30% at T > 650 K and x_s = 20% at T > 400 K. In contrast, the MCYna + LJ calculations yield a single phase at solute concentrations up to 30% for both systems. As the solute particles are modeled by the same LJ potential, the differences observed can be attributed to the water potential. The average MCYna water-water intermolecular energy is –39.0 kJ/mol, which compares with a value of –47.0 kJ/mol for the SPC/E potential. This suggests that the more loosely attracted MCYna water molecules allow solute particles to diffuse inside the hydrogen-bond network to a greater extent than SPC/E water molecules. Differences in the structure of water obtained by the two different potentials are apparent in the oxygen-oxygen RDFs.[35] The SPC/E O–O peak reaches a value 3.2 at T = 298 K while the MCYna O–O peak has a value of 2.5. This again indicates a much more strongly connected water shell structure of the SPC/E model. As shown elsewhere,[35] SPC/E provides better prediction of water's
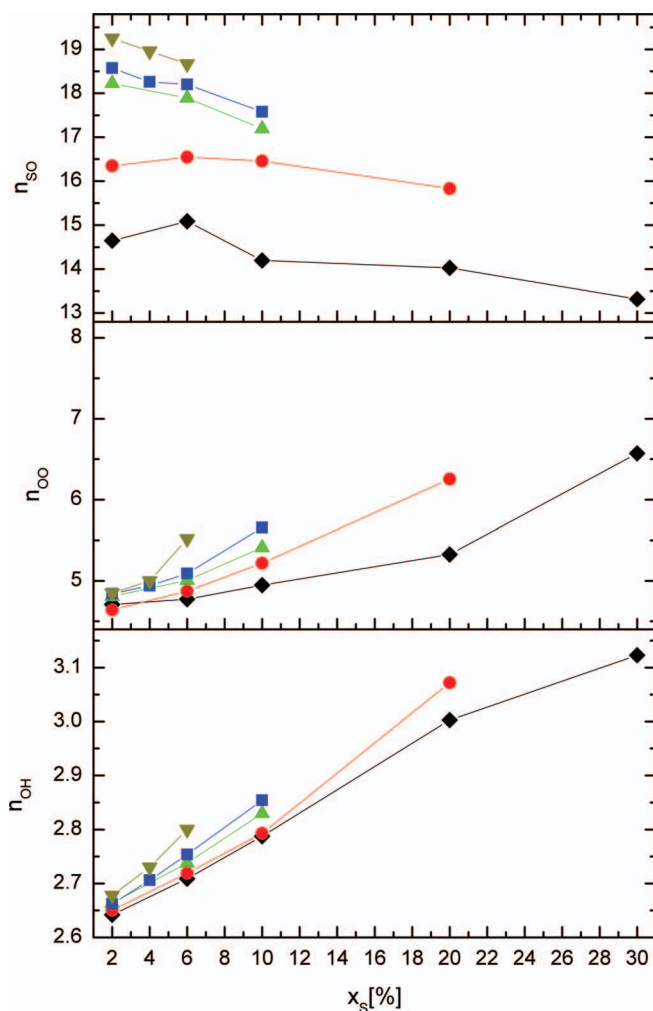
FIG. 5. Coordination numbers of aqueous solutions of Ne (black ◆), Ar (red ●), CH$_4$ (green ▲), Kr (blue ■), and Xe (olive ▼) at T = 298 K as a function of solute concentration. The lines through data points are given only for guidance.

structure at T < 373K, while significantly overestimating its structure at T > 373K, particularly at low densities. The MCYna model underestimates water molecules ordering at ambient conditions, but at the same time, it is much better in predicting the dielectric constant, dipole moment, and to some extent hydrogen bonding (see Figs. 2–4 in the Ref. [35]), which are properties of interest in this work.

C. Structure of the solvation shells

We studied the evolution of water-nonpolar solute solvation shells using the water-Ar system as the example. Aqueous solutions of CH$_4$ and Ne have similar phase behavior at $x_s \leq 30\%$ and exhibit similar temperature dependence of the solvation shells. Figure 4 presents the 1st order coordination numbers for water-argon system calculated by Eq. (11). Since the molecular structure in liquid water differs from a regular configuration of crystal as in ice, it is difficult to unambiguously define a fixed upper limit r_{min} in integral (11). In fact, the coordination number n_{ij} depends largely on the choice of this value. In this work, we accept the position of the first $g_{ij}(r)$ minima as a r_{min}. Thus, r_{min} represents the size of the 1st

solvation shell. Each curve in Fig. 4(a) represents the argon-oxygen coordination number n_{ArO} or the so-called hydration number at different x_s in the one phase region. In general, n_{ArO} slowly decreases with temperature reaching stable values at T ≥ 650 K. At argon percentage mole fractions ≤20% and T < 400 K, the number of water molecules forming a solvation shell around an argon atom is approximately 15∼17 and slowly decreases to 14 at supercritical temperatures. This compares with the hydration values of 15∼14 for water-Ne ($x_s = 20\%$), 16∼17 for water-CH$_4$ ($x_s = 20\%$), 18 for water-Kr ($x_s = 10\%$), and 19∼20 for water-Xe ($x_s = 6\%$). These values lie within the range of hydration numbers reported in the literature.[6,11,31,36]

Oxygen-oxygen coordination numbers n_{oo} for water-argon systems are presented in Fig. 4(b). At temperatures up to the boiling temperature, the presence of Ar atoms increases n_{oo}. For example, the generally accepted value of n_{oo} for pure water at 298 K is 4.6, whereas at $x_s = 10\%$ it is 5.1 and for $x_s = 20\%$ it is 5.96. This increase in the number of water molecules inside the 1st coordination shell can be explained by the formation of a more densely packed H-bond network due to significant repulsion from Ar atoms. Confirmation of this effect is explicitly seen in Fig. 3(b) where the first solute-oxygen peaks at solute concentrations of 20% are clearly higher than that of pure water. This is possible in part because of the incorporation of water molecules from the 2nd shell into the 1st one. Our simulations show that at temperatures up to the boiling temperature, values of n_{oo} at $x_s = 10\%$ are close to n_{oo} of pure water. Naturally, with increasing number of Ar atoms, the tetrahedral water structure becomes increasingly distorted until at some point it collapses completely. By analyzing values of n_{oo} with higher solute concentrations, we can infer that the tetrahedral structure collapses at solute concentrations >20%.

The evolution of the oxygen-hydrogen coordination number (n_{oh}) of the water-argon system is the most interesting one. The O–H coordination numbers for $x_s = 10\%$, 20%, and 30% together with corresponding values for pure water are presented in Fig. 4(c). We have calculated these coordination numbers using Eq. (11) which requires the position of the O–H 1st minima as an upper integration limit. It is important to note that the n_{oh} coordination number is not exactly the number of hydrogen bonds. Equation (11) defines the average number of molecules that are within a distance r_{min} from the central water molecule. As was shown by Kalinichev and Bass,[37] this number coincides with the number of H-bonds only at T ≤ 500 K. At higher temperatures and pressures, more elaborate criteria are required for the definition of H-bonds over a wider range of state points. Nevertheless, n_{oh} can serve as a good approximation of H-bond number, especially at T ≤ 500 K. As we can clearly see from Fig. 4(c), the presence of Ar atoms increase n_{oh}.

Many authors[7,30,31] suggest that small concentrations of inert solutes strengthen the water structure by increasing the number of H-bonds in the first hydration shell. Analyzing the data from Figs. 3(a)–4(c), we can infer that some short-range strengthening of the H-bond network in the vicinity of the solute particle occurs in systems with $x_s \leq 30\%$. However, at the same time, the data from Figs. 3(a) and 3(b) also show

a negative influence of nonpolar solutes on the structuring of water molecules in the second hydration shell, especially at $x_s \geq 20\%$ and at distances larger than 0.4 nm from the solute particle. The n_{oh} values at $x_s = 30\%$, 20%, and 10% are higher than that of pure water at T < 400 K. In the region 400–450 K, a significant drop in n_{oh} is observed and after T = 450 K, all oxygen-hydrogen coordination numbers merge into one and have values that are very close to that of pure water. At T < 400 K, where the tetrahedral structure still exists, the increase in n_{oh} can be explained by the formation of a more densely packed solvation shell due to repulsion from solute atoms. The n_{oh} curve is interrupted at 650 K where the 1st g_{oh} minimum disappears. At this temperature, the 1st and 2nd O–H shells merge and it becomes difficult to unambiguously define a fixed upper limit r_{min} in integral (11). We believe that more than half of the H-bond network breaks at T ≥ 650 K. In the case of $x_s > 30\%$, irrespectively of solute size, the solute particles largely block water molecules from forming either H-bonds or any kind of cluster formations.

Figure 5 presents coordination numbers of water plus Ne, Ar, CH$_4$, Kr, and Xe systems at 298 K as a function of solute concentrations. This figure can be interpreted as the dependence of coordination numbers on the size of the solute particles. All three coordination numbers solute-oxygen, oxygen-oxygen, and oxygen-hydrogen show a clear dependence on the σ parameter of solute particles. Coordination numbers from Fig. 5 follow the dependence $\sigma_{Xe} > \sigma_{Kr} > \sigma_{CH4} > \sigma_{Ar} > \sigma_{Ne}$. This dependence has a very simple explanation; large particles require a large solvation shell whereas small particles require a small shell. n_{oo} and n_{oh} start from values close to that of pure water at small x_s and increase with increasing solute concentrations. In contrast to n_{oo} and n_{oh}, solute-oxygen coordination numbers n_{so} decrease with increasing solute concentrations.

We have compared the internal energies of pure water[17] and water-argon mixtures with argon concentrations 2%, 6%, 10%, and 20% at the same number densities and at T = 298 K. The internal energy of the 2% water-argon system is smaller by –3.181 kJ/mol than that of pure MCYna water. This is in agreement with results from Okazaki *et al.*[31] and Alagona and Tani[30] and indicates the energetic stabilization of vicinal water molecules by solute atoms. However, at slightly higher concentrations, such as $x_s = 6\%$, the water-argon internal energy becomes larger than in pure water, and continues to increase with x_s. This change in internal energy can be explained by the cost of incorporating argon atoms into the H-bond network. Only in very dilute mixtures can the few solute atoms be easily incorporated into the existing water tetrahedral structure without causing significant perturbation. At higher x_s, solute atoms cause more and more perturbations to the structure of water. Despite the somewhat strengthening effect on the 1st surrounding water shell (mainly more dense packing of water molecules), excessive numbers of solute particles destabilize the cohesiveness of the water structure.

D. Dielectric constant

We calculated the dielectric constants ε_m for water plus neon, argon, methane, krypton, and xenon mixtures. For this calculation, we have used the classical fluctuation formula of Kirkwood.[21,26] Despite the fact that the system consists of two molecules, the second molecule is nonpolar and has zero dipole moment. Therefore, only water molecules make a contribution to the total dipole moment of the system used in Eq. (13).

The temperature dependence of the dielectric constants ε_m in the one-phase region for pure water and water plus Ne, Ar, and CH$_4$ systems is presented in Fig. 6. It is apparent, that all values of ε_m gradually decrease with temperature and x_s. The decrease in ε_m with increasing solute concentration is primarily due to solute-hydration effects. For aqueous solutions, the formation of hydration shells around nonpolar solutes prevents the "shell-bounded" water molecules from being oriented in the external field. These water molecules are excluded from creating the effective dipole moment of the system, thus causing a decrease of polarization and dielectric constant. A further increase in solute concentration leads to a water deficit and to a redistribution of water molecules in the hydration layers. Despite the significant difference in the Ne, Ar, and CH$_4$ size and energy parameters, the dielectric constants of these three systems are almost identical for a given temperature and x_s. The difference in ε_m values is within ±1%–1.5%.

The absence of experimental data for the dielectric properties of water-nonpolar solute systems makes it impossible to validate the predictions of the MCYna + LJ potential. However, it has been previously reported[35] that the MCYna potential provides a good prediction of the dielectric properties of pure water over a wide range of temperatures. The discrepancy between simulations[35] and experiment was typically 5%, which suggests that we can have a reasonable degree of confidence in the reliability of the mixture calculations.

Figure 7 presents dielectric constants ε_m for the various water mixtures as functions of x_s at T = 298 K. In general, the dielectric constants decrease with increasing concentration of the solute. It is natural to expect values of ε_m for very dilute mixtures ($x_s < 2\%$) to be very close to that of pure water. Indeed examining Fig. 7 in the direction of decreasing solute concentration x_s, we can clearly see that the values of ε_m for all mixtures converge to the dielectric constant value of pure water ($x_s = 0\%$) at 298 K. It is noteworthy that there is a small but nevertheless noticeable peak at approximately $x_s = 1\%$ for mixtures containing either krypton, or xenon. While more extensive simulations are always preferable for better convergence of the dielectric constant, this observation may be directly connected with the nature of the hydrophobic hydration of krypton and xenon. As was elaborated by Chandler,[38] solvation of the single particles, which excludes water molecules from a spherical volume less than 0.5 nm across, does not require the breaking of hydrogen bonds. Water molecules can adopt orientations that allow hydrogen-bonding patterns to go around the solute in such single cavities. Therefore, at very dilute concentrations, large nonpolar particles such as krypton and xenon enhance local water ordering, which may lead to a small increase in dielectric constant and dipole moment. Enhanced local water ordering in dilute solutions has also been observed by Cristofori *et al.*[11] and Okazaki *et al.*[31] The situation is different for x_s
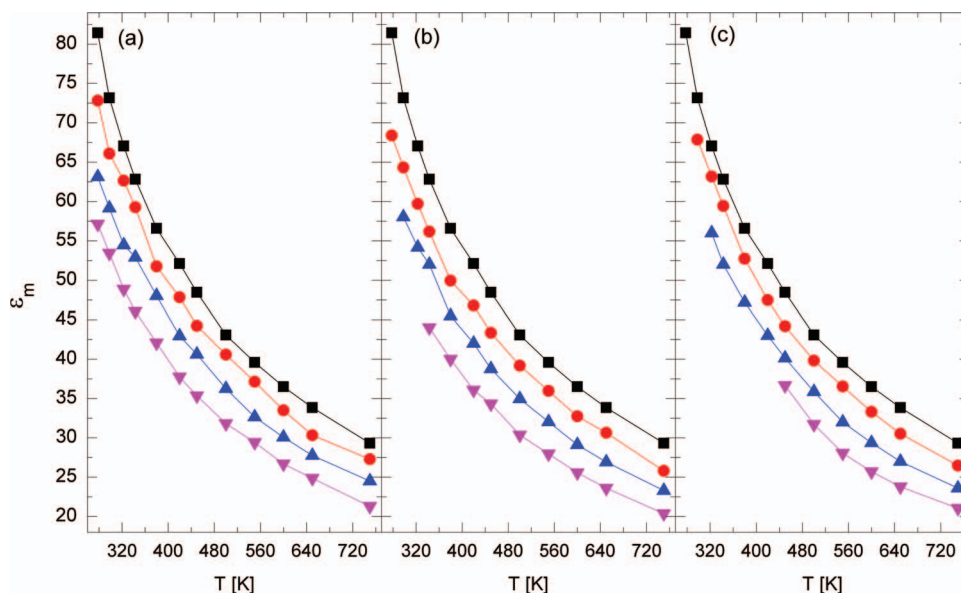
FIG. 6. Temperature dependence of the dielectric constants of (a) water-Ne, (b) water-Ar, and (c) water-CH$_4$ systems at solute concentrations 0% (black ■), 10% (red ●), 20% (blue ▲), and 30% (pink ▼). The lines through data points are given only for guidance.

> 2% where solute particles tend to aggregate, forming large hydrophobic cavities with low curvature, making it impossible for water molecules to maintain a complete hydrogen-bonding network.

E. Comparison of MD and analytical calculations of dielectric constants

It is of interest to compare the dielectric constants for the water + methane mixture predicted by the combined MCYna + LJ potential with the results obtained using simple analytical mixing rules developed by Harvey and Prausnitz[39] and other empirical formulas.[40] The Harvey-Prausnitz linear and quadratic mixing rules are based on the calculation of pure components polarizations $p_i^\pm$ obtained at the reduced density

FIG. 7. Dielectric constants of aqueous solutions of Ne (black ◆), Ar (red ●), CH$_4$ (green ▲), Kr (blue ■), and Xe (olive ▼) at T = 298 K as functions of solutes concentration. The lines through data points are given only for guidance.

of the mixture, insuring that all molar volumes are physically appropriate,

$$p_m = \sum_{i=1}^{n} \Phi_i^\pm p_i^\pm. \tag{16}$$

A quadratic mixing rule was developed to account for increased or decreased degree of correlation between neighboring molecules in the mixture,

$$p_m = \sum_{i=1}^{n} \sum_{j}^{n} \Phi_i^\pm \Phi_j^\pm p_{ij}^\pm, \tag{17}$$

where $p_{ij}^\pm = \frac{1}{2}(p_i^\pm + p_j^\pm)\xi$. ξ is an adjustable parameter used to optimize agreement between theory and experiment. Analysis of the binary mixture critical curve indicates[41] that a value of $\xi = 0.92$ is appropriate for methane + water interactions. The dielectric constant of the mixture ε_m is obtained from Kirkwood's expression for polar fluids

$$p_m = \frac{(\varepsilon_m - 1)(2\varepsilon_m + 1)}{9\varepsilon_m}. \tag{18}$$

We also investigated several empirical rules attributed by van Beek[40] to Looyenga, Lichtenecker, Bruggeman, Böttcher, and Rayleigh. Of the various alternatives summarized by van Beek,[40] we found that the Rayleigh formula yielded values of ϵ_m closest to our MD simulations. The Rayleigh formula is

$$\varepsilon_m = \varepsilon_1 \frac{\frac{2\varepsilon_1 + \varepsilon_2}{\varepsilon_2 - \varepsilon_1} + 2V_2 - \frac{1.575(\varepsilon_2 - \varepsilon_1)}{4\varepsilon_1 + 3\varepsilon_2} V_2^{10/3}}{\frac{2\varepsilon_1 + \varepsilon_2}{\varepsilon_2 - \varepsilon_1} - V_2 - \frac{1.575(\varepsilon_2 - \varepsilon_1)}{4\varepsilon_1 + 3\varepsilon_2} V_2^{10/3}}, \tag{19}$$

where V_2 is the dimensionless fractional volume of the dispersed (solute) component. The derivation of Eq. (19) assumes a cubical array of spheres (ε_2) enclosed in a medium (ε_1), which appears to be a reasonable approximation for methane in water. Furthermore, the dielectric constants of methane and noble gases at T > 278 K are very close to 1
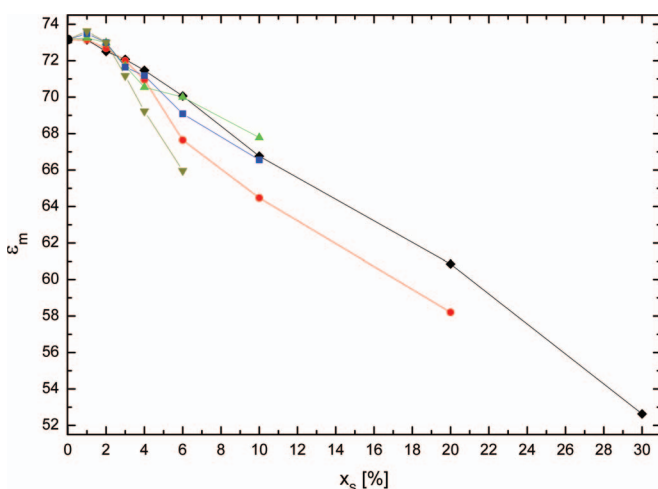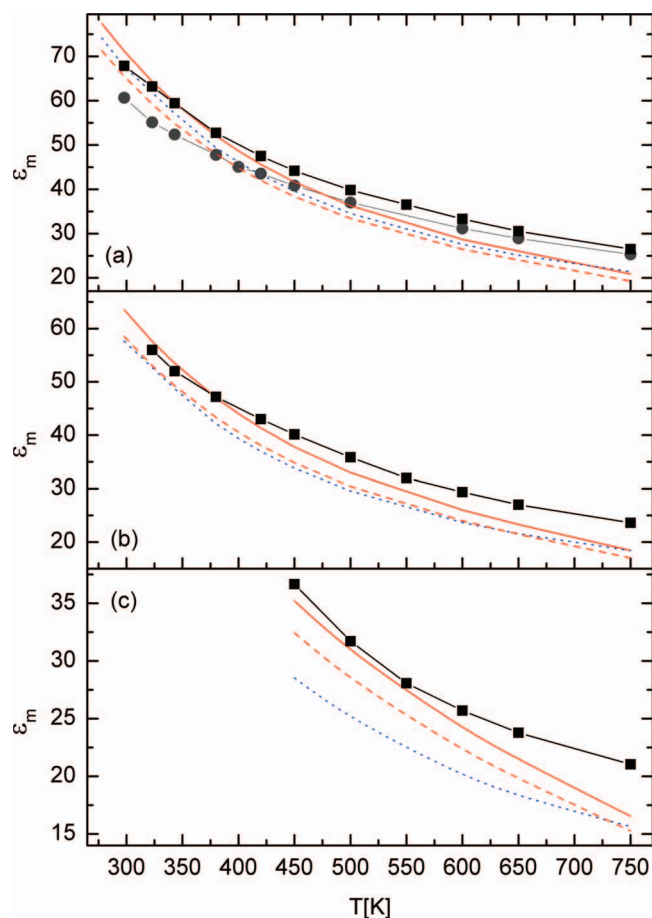
FIG. 8. Comparison of the dielectric constants of the water-CH$_4$ (c) system at solute concentrations (a) 10%, (b) 20%, and (c) 30% obtained from MD simulations of MCYna + LJ model (■), SPC/E + LJ model (●), linear mixing rule Eq. (16) (continuous red line), quadratic mixing rule Eq. (17) (dashed red line), and Eq. (19) (dotted blue line). The lines through data points are given only for guidance.

so it is natural to expect very small contribution to the total dielectric constant of the mixture from the solute component. For example, according to the Harvey-Prausnitz approach, at $x_s = 10\%$ and T < 373 K, methane contributes less than 1% to the total dielectric constant of the mixture and it makes an even smaller contribution at higher temperatures.

It is important to note that particles such as methane and xenon have relatively high electronic polarizabilities of 2.6 and 4.11 Å^3, respectively. Some authors[25,42] suggest that single methane molecules can acquire a small induced dipole moment upon hydration, which can affect the solvation process and consequently dielectric constant of the mixture. However, Mateus et al.[25] found no difference between the average monomeric dipole moment of bulk water and that of water in close interaction (within the first hydration layer) with methane. A proper account of solute polarizability requires a thorough *ab initio* approach and is beyond the scope of the present study.

Comparison of the ε_m from the given polarizable potential model with the Harvey-Prausnitz mixing rules, Rayleigh's formula, and non-polarizable SPC/E + LJ potential model for the water-methane system at methane concentrations 10%, 20%, and 30% is presented in Fig. 8. This comparison indicates that Eq. (16) with linear volume-fraction mixing at $x_s = 10\%$ and 20% slightly overestimates ε_m at T < 343 and 370 K, respectively. At higher temperatures, all analytical formulae underestimate ε_m. The quadratic mixing rule (17) and Rayleigh's Eq. (19) underestimate MD results for all temperatures and solute concentrations. One of the reasons for this difference between MD and analytical results at elevated temperatures is the quite high dipole moment of the MCYna water molecule, which contributes to ε of pure water higher by 5% compared to experimental data. Deviation between MD data and the quadratic mixing rule Eq. (17) can be explained by the fact that this rule was developed to improve agreement over the linear rule for water-alcohol systems. These systems
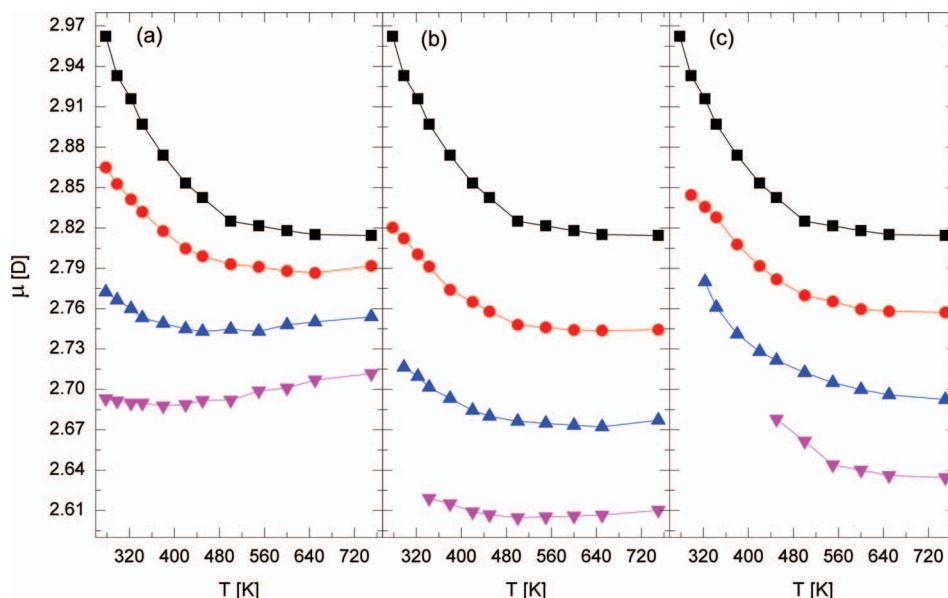

FIG. 9. Temperature dependence of the average dipole moments of (a) water-Ne, (b) water-Ar, and (c) water-CH$_4$ systems at solute concentrations 0% (black ■), 10% (red ●), 20% (blue ▲), and 30% (pink ▼). The lines through data points are given only for guidance.
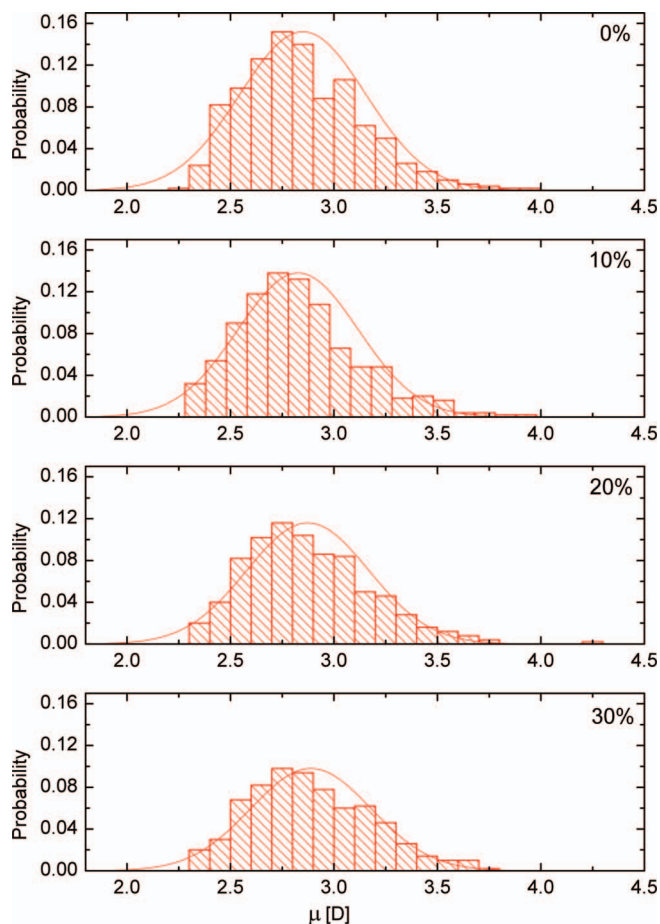
FIG. 10. Instantaneous snapshots of the distribution of dipole moments for the water-CH_4 system at T = 450 K and solute concentrations of 0%, 10%, 20%, and 30%. Smooth curves show corresponding Gaussian distributions.

are fully soluble and possess stronger correlation between the neighboring molecules, which is obviously not the case for hydrophobic solutes such as methane or noble gases. In general, we can conclude that the Harvey-Prausnitz linear mixing rule and the predictions of MCYna + LJ model are in a qualitative agreement at all temperatures and solute concentrations.

F. Dipole moment

Figure 9 shows the temperature dependence of the average water molecule dipole moment μ_m at different mole fractions of water plus Ne, Ar, and CH_4 systems. At temperatures up to 500 K, all dipoles slowly decrease, while at higher temperatures, dipoles of water-Ar and water-CH_4 systems are almost constant. In contrast to Ar and CH_4 mixtures, dipole moments of the water-Ne system at supercritical temperatures exhibit small but steady increases. Values of μ_m for the given systems differ much more than in the case of dielectric constants. For example, μ_m of the water-CH_4 system are clearly higher than μ_m of water-Ar system, and the difference increases with x_s, from 1% for $x_s = 10\%$ to 2.5% for $x_s = 30\%$. Dipoles for water-Ne system appear to be higher than for Ar and CH_4 and the distance between the curves of constant x_s is smaller. A possible explanation of this weak deviation of water-Ne system dipoles from pure water could be partly attributed to the parameters used for Ne. The Lennard-Jones parameters $\sigma = 0.3035$ nm and especially $\varepsilon/k_b = 18.56$ K from Table II appear to be disproportionally small compared to Ar, CH_4, Kr, and Xe. Having such a small ε, which basically defines the depth of the LJ potential well, means that Ne atoms interact very weakly with water molecules.

Figure 10 shows the probability distribution of individual dipole moments at T = 450 K for pure MCYna water and water-methane systems with $x_s = 10\%$, 20%, and 30%. These
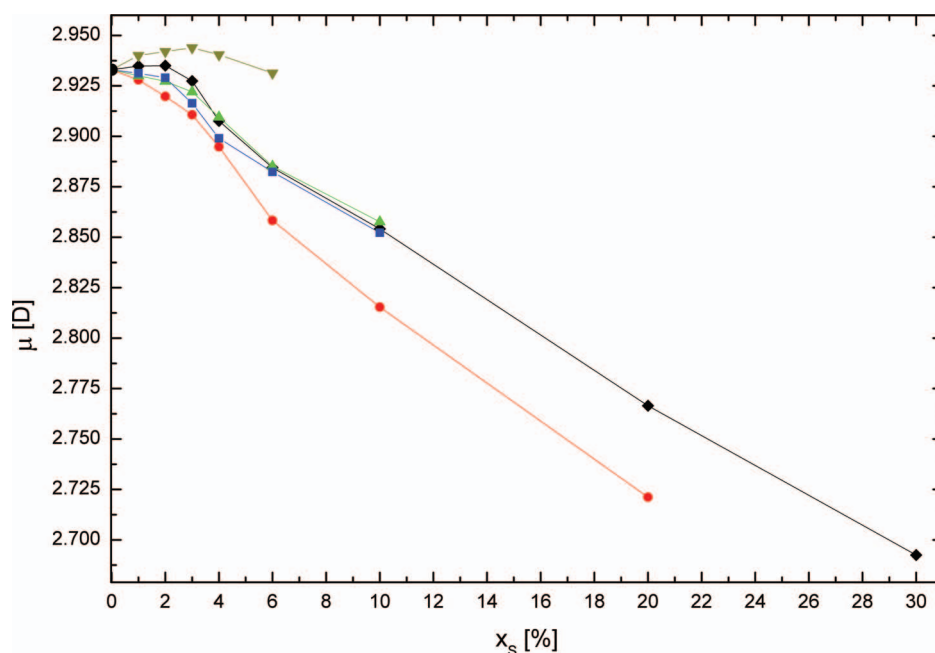

FIG. 11. Average dipole moments of aqueous solutions of Ne (black ◆), Ar (red ●), CH_4 (green ▲), Kr (blue ■), and Xe (olive ▼) at T = 298 K as a function of solute concentration. The lines through data points are given only for guidance.

distributions were obtained from an instantaneous snapshot at the end of the simulation. Deviation from the Gaussian distribution reflects local fluctuation of molecular dipole at the given instance. From this figure, we can see that the mean values, height, and width of the distributions gradually decrease with increasing x_s. In accordance with Fig. 9, the mean values of the distributions become progressively shifted to the left with increasing concentration. This dependence seems to have a simple explanation. Namely, the neutral solute particles especially at high concentrations repel water molecules and weaken the intermolecular electric field. As a consequence, at decreasing electric field, the induction contribution μ_{ind} to the total molecular dipole moment is also vanishing. Dipole distributions for water-Ne and water-Ar systems show the same behavior.

The concentration dependence of the dipole moments of water mixtures at T = 298 K is illustrated in Fig. 11. In common with the dielectric constants (Fig. 7), the average dipole moment decreases with increasing solute concentration. We observe a distinct peak in the dipole moment at $x_s < 3\%$ for the water-xenon curve and a slight increase for the water-neon curve. The reason for the small increase of the average dipole moment in the presence of xenon atoms is the same as it was for the dielectric constant, namely, local strengthening of the water structure. The small deviation of the water-neon properties from the general trend can probably be attributed to the less accurate parameterization of the neon potential due to quantum influences. Excluding the water-neon mixture, the dipole moments of the mixtures exhibit a dependency on the size of the solute as judged by the size of the σ parameter (Table II). The dipole moment is larger in mixtures with larger solutes. That is, μ_m values decrease in the following order: Xe > CH$_4$/Kr > Ar.

IV. CONCLUSIONS

In this work, we have examined the structural, dielectric, and polarization properties of different water-nonpolar solute systems in the single-phase region. A combined MCYna + LJ potential was chosen for these systems with Lorentz-Berthelot combining rules. The MCYna + LJ model reproduces the experimentally observed homogeneous phase region of both water-methane and water-noble gas systems more accurately than the SPC/E + LJ model. At solute percentage mole fractions $x_s \leq 30\%$, some strengthening of vicinal water structure was observed. This strengthening is manifested mainly by increasing numbers of water molecules in the 1st solvation shell around solute particles and consequent increases in the O–O and O–H coordination numbers. At $x_s > 30\%$, excessive number of solute particles starts to play a destructive role on water's tetrahedral structure, preventing water molecules from forming H-bonds. Coordination numbers follow the same dependence as the parameter σ, $\sigma_{Xe} > \sigma_{Kr} > \sigma_{CH4} > \sigma_{Ar} > \sigma_{Ne}$. The n_{oo} and n_{oh} start from values close to that of pure water at small x_s and increase with increasing solute concentrations. In contrast to n_{oo} and n_{oh}, solute-oxygen coordination numbers decrease with increasing solute concentrations.

The dielectric constant ε_m and average dipole moment μ_m of water-nonpolar solute systems have been calculated. The calculations confirmed the gradual decrease of dielectric constant and average dipole moment with temperature and solute concentration. At high temperatures, this trend is caused by the reduction of polarizability of the system, which in turn is caused by the collapse of the H-bond network and resulting thermal fluctuations that oppose dipole alignment by an electrostatic field. In case of high solute concentration, the trend is caused by the "negative" influence of solute particles on cooperative response of water molecules on the external field. Dielectric constants ε_m calculated in the given MD simulation are in good agreement with the analytical approach of calculating ε_m of aqueous solutions (see Eq. (16)) at small solute concentrations x_s and temperatures up to the boiling temperature of water. At higher temperatures and solute concentrations, analytical calculations underestimate ε_m compared to MD results.

[1]G. Wu, M. Heilig, H. Lentz, and E. U. Franck, Ber. Bunsenges. Phys. Chem. **94**, 24 (1990).

[2]E. U. Franck, H. Lentz, and H. Welsch, Z. Phys. Chem., Neue. Folge **93**, 95 (1974).

[3]M. L. Japas and E. U. Franck, Ber. Bunsenges. Phys. Chem. **89**, 793 (1985).

[4]J. R. Errington, G. C. Boulougouris, I. G. Economou, A. Z. Panagiotopoulos, and D. N. Theodorou, J. Phys. Chem. B **102**, 8865 (1998).

[5]D. M. Sullivan, G. W. Neilson, and H. E. Fischer, J. Chem. Phys. **115**, 339 (2001).

[6]A. Botti, F. Bruni, A. Isopo, G. Modesti, C. Oliva, M. A. Ricci, R. Senesi, and A. K. Soper, J. Chem. Phys. **118**, 235 (2003).

[7]B. Guillot and Y. Guissani, J. Chem. Phys. **99**, 8075 (1993).

[8]V. De Grandis, P. Gallo, and M. Rovere, J. Chem. Phys. **118**, 3646 (2003).

[9]A. Ben-Naim, J. Chem. Phys. **90**, 7412 (1989).

[10]R. M. Lynden-Bell and J. C. Rasaiah, J. Chem. Phys. **107**, 1981 (1997).

[11]P. Cristofori, P. Gallo, and M. Rovere, Mol. Phys. **103**, 501 (2005).

[12]H. J. C. Berendsen, J. R. Grigera, and T. P. Straatsma, J. Phys. Chem. **91**, 6269 (1987).

[13]P. M. Rodger, J. Phys. Chem. **94**, 6080 (1990).

[14]L. Poling, Science **134**, 15 (1961).

[15]P. J. Dyer, H. Docherty, and P. T. Cummings, J. Chem. Phys. **129**, 024508 (2008).

[16]O. Matsuoka, E. Clementi, and M. Yoshimine, J. Chem. Phys. **64**, 1351 (1976).

[17]J. Li, Z. Zhou, and R. J. Sadus, J. Chem. Phys. **127**, 154509 (2007).

[18]G. Marcelli and R. J. Sadus, J. Chem. Phys. **111**, 1533 (1999).

[19]B. M. Axilrod and E. Teller, J. Chem. Phys. **11**, 299 (1943).

[20]P. J. Leonard and J. A. Barker, in *Theoretical Chemistry: Advances and Perspectives*, edited by H. Eyring and D. Henderson (Academic, London, 1975), Vol. 1.

[21]C. G. Gray and K. E. Gubbins, *Theory of Molecular Fluids* (Clarendon, Oxford, 1984), Vol. 1.

[22]M. Losonczy, J. W. Moskowitz, and F. H. Stillinger, J. Chem. Phys. **59**, 3264 (1973).

[23]G. Chałasiński, M. M. Szczęśniak, and S. Scheiner, J. Chem. Phys. **94**, 2807 (1991).

[24]M. M Szczęśniak, G. Chałasiński, S. M. Cybulsku, and P. Cieplak, J. Chem. Phys. **98**, 3078 (1993).

[25]M. P. S. Mateus, N. Galamba, B. J. C. Cabral, K. Coutinho, and S. Canuto, Chem. Phys. Lett. **506**, 183 (2011).

[26]R. J. Sadus, *Molecular Simulation of Fluids: Theory, Algorithms and Object-Orientation* (Elsevier, Amsterdam, 1999).

[27] M. S. Skaf and B. M. Ladanyi, J. Chem. Phys. **102**, 6542 (1995).

[28] M. Neumann, Mol. Phys. **50**, 841 (1983).

[29] G. Karniadakis and R. M. Kirby, *Parallel Scientific Computing in C and MPI: A Seamless Approach to Parallel Algorithms and their Implementation* (Cambridge University Press, Cambridge, 2003).

[30] G. Alagona and A. Tani, J. Chem. Phys. **72**, 580 (1980).

[31] S. Okazaki, K. Nakanishi, H. Touhara, and Y. Adachi, J. Chem. Phys. **71**, 2421 (1979).

[32] E. U. Franck, Pure Appl. Chem. **59**, 25 (1987).

[33] H. Zheng, T. Duan, and Q. Sun, Exp. Therm. Fluid Sci. **38**, 262 (2012).

[34] O. L. Culberson and J. J. McKetta, Jr., Trans. Am. Inst. Min., Metall Pet. Eng. **192**, 223 (1951).

[35] I. Shvab, and R. J. Sadus, Phys. Rev. E **85**, 051509 (2012).

[36] S. F. Dec, K. E. Bowler, L. L. Stadterman, C. A. Koh, and E. D. Sloan, Jr., J. Am. Chem. Soc. **128**, 414 (2006).

[37] A. G. Kalinichev and J. D. Bass, Chem. Phys. Lett. **231**, 301 (1994).

[38] D. Chandler, Nature (London) **437**, 640 (2005).

[39] A. H. Harvey and J. M. Prausnitz, J. Solution Chem. **16**, 857 (1987).

[40] L. K. H. Van Beek, *Progress in Dielectrics* (Heywood, London, 1967), Vol. 7.

[41] V. M. Shmonov, R. J. Sadus, and E. U. Franck, J. Phys. Chem. **97**, 9054 (1993).

[42] L. Rossato, F. Rossetto, and P. L. Silvestrelli, J. Phys. Chem. B **116**, 4552 (2012).